



# Triple cation mixed-halide perovskites for tunable lasers

PHILIPP BRENNER,<sup>1,\*</sup> TIM GLÖCKLER,<sup>1</sup> DIANA RUEDA-DELGADO,<sup>1</sup> TOBIAS ABZIEHER,<sup>1</sup> MARIUS JAKOBY,<sup>2</sup> BRYCE S. RICHARDS,<sup>1,2</sup> ULRICH W. PAETZOLD,<sup>1,2</sup> IAN A. HOWARD,<sup>1,2</sup> AND ULI LEMMER<sup>1,2</sup>

<sup>1</sup>Light Technology Institute, Karlsruhe Institute of Technology, 76131 Karlsruhe, Germany

<sup>2</sup>Institute of Microstructure Technology, Karlsruhe Institute of Technology, 76344 Eggenstein-Leopoldshafen, Germany

\*philipp.brenner@kit.edu

**Abstract:** Metal halide perovskites are recently attracting strong attention due to their potential in solar cells, LEDs, and lasers. Here, we demonstrate the broad spectral tuning of the optical gain characteristics of triple cation (containing methylammonium, formamidinium and cesium) mixed-halide perovskite thin films. We explicitly study the interrelation between amplified spontaneous emission (ASE) thresholds, the operational stability of the gain, and the material composition. The incorporation of cesium and a deficiency of lead in the precursor solutions is found to be crucial for low ASE thresholds and the improved stability of mixed-halide perovskites. We tune the photoluminescence in mixed-halide perovskites between peak wavelengths of 510 and 790 nm by exchanging the halide from iodide to bromide and chloride in small steps of 10%, while preserving the narrowband emission below a linewidth of 130 meV for all mixtures. The optical gain under ns-excitation can be tuned over a significant portion of this spectral window; we observe ASE emission in regions between 545 to 555 nm and 680 to 810 nm. This is a significant step towards perovskite lasers operating through a broad portion of the visible to near infrared spectrum.

© 2017 Optical Society of America

**OCIS codes:** (160.3380) Laser materials; (160.4670) Optical materials; (130.5990) Semiconductors; (160.6000) Semiconductor materials; (160.4236) Nanomaterials.

## References and links

1. S. Kazim, M. K. Nazeeruddin, M. Grätzel, and S. Ahmad, "Perovskite as Light Harvester: A Game Changer in Photovoltaics," *Angew. Chem. Int. Ed. Engl.* **53**(11), 2812–2824 (2014).
2. S. D. Stranks and H. J. Snaith, "Metal-halide perovskites for photovoltaic and light-emitting devices," *Nat. Nanotechnol.* **10**(5), 391–402 (2015).
3. See <https://www.nrel.gov/pv>, "Research Cell Efficiency record chart by the National Renewable Energy Laboratory, Accessed on 22 July 2017.
4. B. R. Sutherland and E. H. Sargent, "Perovskite photonic sources," *Nat. Photonics* **10**(5), 295–302 (2016).
5. M. Saba, M. Cadelano, D. Marongiu, F. Chen, V. Sarritzu, N. Sestu, C. Figus, M. Aresti, R. Piras, A. G. Lehmann, C. Cannas, A. Musinu, F. Quochi, A. Mura, and G. Bongiovanni, "Correlated electron-hole plasma in organometal perovskites," *Nat. Commun.* **5**, 5049 (2014).
6. S. Chénais and S. Forget, "Recent advances in solid-state organic lasers," *Polym. Int.* **61**(3), 390–406 (2012).
7. S. Z. Bisri, T. Takenobu, and Y. Iwasa, "The pursuit of electrically-driven organic semiconductor lasers," *J. Mater. Chem. C Mater. Opt. Electron. Devices* **2**(16), 2827 (2014).
8. P. Brenner, L. M. Fleig, X. Liu, A. Welle, S. Bräse, and U. Lemmer, "Degradation mechanisms of polyfluorene-based organic semiconductor lasers under ambient and oxygen-free conditions," *J. Polym. Sci. Part B Polym. Phys.* **53**, 1029–1034 (2015).
9. J. Q. Grim, S. Christodoulou, F. Di Stasio, R. Krahn, R. Cingolani, L. Manna, and I. Moreels, "Continuous-wave biexciton lasing at room temperature using solution-processed quantum wells," *Nat. Nanotechnol.* **9**(11), 891–895 (2014).
10. F. Fan, O. Voznyy, R. P. Sabatini, K. T. Bicanic, M. M. Adachi, J. R. McBride, K. R. Reid, Y.-S. Park, X. Li, A. Jain, R. Quintero-Bermudez, M. Saravanapavanantham, M. Liu, M. Korkusinski, P. Hawrylak, V. I. Klimov, S. J. Rosenthal, S. Hoogland, and E. H. Sargent, "Continuous-wave lasing in colloidal quantum dot solids enabled by facet-selective epitaxy," *Nature* **544**(7648), 75–79 (2017).
11. Z. Yang, M. Pelton, I. Fedin, D. V. Talapin, and E. Waks, "A room temperature continuous-wave nanolaser

- using colloidal quantum wells,” *Nat. Commun.* **8**(1), 143 (2017).
12. A. S. D. Sandanayaka, T. Matsushima, F. Bencheikh, K. Yoshida, M. Inoue, T. Fujihara, K. Goushi, J.-C. Ribierre, and C. Adachi, “Toward continuous-wave operation of organic semiconductor lasers,” *Sci. Adv.* **3**(4), e1602570 (2017).
  13. G. Li, M. Price, and F. Deschler, “Research Update: Challenges for high-efficiency hybrid lead-halide perovskite LEDs and the path towards electrically pumped lasing,” *APL Mater.* **4**(9), 091507 (2016).
  14. Q. Zhang, R. Su, W. Du, X. Liu, L. Zhao, S. T. Ha, and Q. Xiong, “Advances in Small Perovskite-Based Lasers,” *Small Methods* **1**(9), 1700163 (2017).
  15. S. A. Veldhuis, P. P. Boix, N. Yantara, M. Li, T. C. Sum, N. Mathews, and S. G. Mhaisalkar, “Perovskite Materials for Light-Emitting Diodes and Lasers,” *Adv. Mater.* **28**(32), 6804–6834 (2016).
  16. I. Suárez Alvarez, “Active photonic devices based on colloidal semiconductor nanocrystals and organometallic halide perovskites,” *Eur. Phys. J. Appl. Phys.* **75**(3), 30001 (2016).
  17. G. Xing, N. Mathews, S. S. Lim, N. Yantara, X. Liu, D. Sabba, M. Grätzel, S. Mhaisalkar, and T. C. Sum, “Low-temperature solution-processed wavelength-tunable perovskites for lasing,” *Nat. Mater.* **13**(5), 476–480 (2014).
  18. R. Dhanker, A. N. Brigeman, A. V. Larsen, R. J. Stewart, J. B. Asbury, and N. C. Giebink, “Random lasing in organo-lead halide perovskite microcrystal networks,” *Appl. Phys. Lett.* **105**(15), 151112 (2014).
  19. Q. Zhang, S. T. Ha, X. Liu, T. C. Sum, and Q. Xiong, “Room-Temperature Near-Infrared High-Q Perovskite Whispering-Gallery Planar Nano lasers,” *Nano Lett.* **14**(10), 5995–6001 (2014).
  20. B. R. Sutherland, S. Hoogland, M. M. Adachi, C. T. O. Wong, and E. H. Sargent, “Conformal organohalide perovskites enable lasing on spherical resonators,” *ACS Nano* **8**(10), 10947–10952 (2014).
  21. S. Yakunin, L. Protesescu, F. Krieg, M. I. Bodnarchuk, G. Nedelcu, M. Humer, G. De Luca, M. Fiebig, W. Heiss, and M. V. Kovalenko, “Low-threshold amplified spontaneous emission and lasing from colloidal nanocrystals of caesium lead halide perovskites,” *Nat. Commun.* **6**, 8056 (2015).
  22. P. J. Cegielski, S. Neutzner, C. Porschatis, H. Lerch, J. Bolten, S. Suckow, A. R. S. Kandada, B. Chmielak, A. Petrozza, T. Wahlbrink, and A. L. Giesecke, “Integrated perovskite lasers on a silicon nitride waveguide platform by cost-effective high throughput fabrication,” *Opt. Express* **25**(12), 13199–13206 (2017).
  23. P. Brenner, M. Stulz, D. Kapp, T. Abzieher, U. W. Paetzold, A. Quintilla, I. A. Howard, H. Kalt, and U. Lemmer, “Highly stable solution processed metal-halide perovskite lasers on nanoimprinted distributed feedback structures,” *Appl. Phys. Lett.* **109**(14), 141106 (2016).
  24. Y. Jia, R. A. Kerner, A. J. Grede, A. N. Brigeman, B. P. Rand, and N. C. Giebink, “Diode-pumped organo-lead halide perovskite lasing in a metal-clad distributed feedback resonator,” *Nano Lett.* **16**(7), 4624–4629 (2016).
  25. G. L. Whitworth, J. R. Harwell, D. N. Miller, G. J. Hedley, W. Zhang, H. J. Snaith, G. A. Turnbull, and I. D. W. Samuel, “Nanoimprinted distributed feedback lasers of solution processed hybrid perovskites,” *Opt. Express* **24**(21), 23677–23684 (2016).
  26. F. Deschler, M. Price, S. Pathak, L. E. Klintberg, D. D. Jarausch, R. Higler, S. Hüttner, T. Leijtens, S. D. Stranks, H. J. Snaith, M. Atatüre, R. T. Phillips, and R. H. Friend, “High Photoluminescence Efficiency and Optically Pumped Lasing in Solution-Processed Mixed Halide Perovskite Semiconductors,” *J. Phys. Chem. Lett.* **5**(8), 1421–1426 (2014).
  27. S. Chen, C. Zhang, J. Lee, J. Han, and A. Nurmikko, “High-Q, Low-Threshold Monolithic Perovskite Thin-Film Vertical-Cavity Lasers,” *Adv. Mater.* **29**(16), 1604781 (2017).
  28. S. Chen, K. Roh, J. Lee, W. K. Chong, Y. Lu, N. Mathews, T. C. Sum, and A. Nurmikko, “A Photonic Crystal Laser from Solution Based Organo-Lead Iodide Perovskite Thin Films,” *ACS Nano* **10**(4), 3959–3967 (2016).
  29. N. Pourdavoud, S. Wang, A. Mayer, T. Hu, Y. Chen, A. Marianovich, W. Kowalsky, R. Heiderhoff, H. C. Scheer, and T. Riedl, “Photonic Nanostructures Patterned by Thermal Nanoimprint Directly into Organo-Metal Halide Perovskites,” *Adv. Mater.* **29**(12), 1605003 (2017).
  30. M. Cadelano, V. Sarritzu, N. Sestu, D. Marongiu, F. Chen, R. Piras, R. Corpino, C. M. Carbonaro, F. Quochi, M. Saba, A. Mura, and G. Bongiovanni, “Can Trihalide Lead Perovskites Support Continuous Wave Lasing?” *Adv. Opt. Mater.* **3**(11), 1557–1564 (2015).
  31. E. T. Hoke, D. J. Slotcavage, E. R. Dohner, A. R. Bowring, H. I. Karunadasa, and M. D. McGehee, “Reversible photo-induced trap formation in mixed-halide hybrid perovskites for photovoltaics,” *Chem. Sci. (Camb.)* **6**(1), 613–617 (2015).
  32. S. J. Yoon, S. Draguta, J. S. Manser, O. Sharia, W. F. Schneider, M. Kuno, and P. V. Kamat, “Tracking Iodide and Bromide Ion Segregation in Mixed Halide Lead Perovskites during Photoirradiation,” *ACS Energy Lett.* **1**(1), 290–296 (2016).
  33. M. Hu, C. Bi, Y. Yuan, Y. Bai, and J. Huang, “Stabilized wide bandgap MAPbBr<sub>3-x</sub>I<sub>3-x</sub> perovskite by enhanced grain size and improved crystallinity,” *Adv Sci (Weinh)* **3**(6), 1500301 (2016).
  34. J. T. Jacobsson, J. P. Correa Baena, M. Pazoki, M. Saliba, K. Schenk, M. Grätzel, and A. Hagfeldt, “An exploration of the compositional space for mixed lead halogen perovskites for high efficiency solar cells,” *Energy Environ. Sci.* **9**(5), 1706–1724 (2016).
  35. M. Saliba, T. Matsui, J.-Y. Seo, K. Domanski, J.-P. Correa-Baena, M. K. Nazeeruddin, S. M. Zakeeruddin, W. Tress, A. Abate, A. Hagfeldt, and M. Grätzel, “Cesium-containing triple cation perovskite solar cells: improved stability, reproducibility and high efficiency,” *Energy Environ. Sci.* **9**(6), 1989–1997 (2016).
  36. L. M. Herz, “Charge-Carrier Dynamics in Organic-Inorganic Metal Halide Perovskites,” *Annu. Rev. Phys. Chem.* **67**(1), 65–89 (2016).
  37. D. Bi, W. Tress, M. I. Dar, P. Gao, J. Luo, C. Renevier, K. Schenk, A. Abate, F. Giordano, J. P. Correa Baena, J.

- D. Decoppet, S. M. Zakeeruddin, M. K. Nazeeruddin, M. Grätzel, and A. Hagfeldt, "Efficient luminescent solar cells based on tailored mixed-cation perovskites," *Sci. Adv.* **2**(1), e1501170 (2016).
38. T. J. Jacobsson, J. P. Correa-Baena, E. Halvani Anaraki, B. Philippe, S. D. Stranks, M. E. F. Bouduban, W. Tress, K. Schenk, J. Teuscher, J. E. Moser, H. Rensmo, and A. Hagfeldt, "Unreacted  $\text{PbI}_2$  as a Double-Edged Sword for Enhancing the Performance of Perovskite Solar Cells," *J. Am. Chem. Soc.* **138**(32), 10331–10343 (2016).
39. L. Qin, L. Lv, Y. Ning, C. Li, Q. Lu, L. Zhu, Y. Hu, Z. Lou, F. Teng, and Y. Hou, "Enhanced amplified spontaneous emission from morphology-controlled organic–inorganic halide perovskite films," *RSC Advances* **5**(125), 103674 (2015).
40. F. Liu, Q. Dong, M. K. Wong, A. B. Djurišić, A. Ng, Z. Ren, Q. Shen, C. Surya, W. K. Chan, J. Wang, A. M. C. Ng, C. Liao, H. Li, K. Shih, C. Wei, H. Su, and J. Dai, "Is Excess  $\text{PbI}_2$  Beneficial for Perovskite Solar Cell Performance?" *Adv. Energy Mater.* **6**(7), 1–9 (2016).
41. G. E. Eperon, S. D. Stranks, C. Menelaou, M. B. Johnston, L. M. Herz, and H. J. Snaith, "Formamidinium lead trihalide: a broadly tunable perovskite for efficient planar heterojunction solar cells," *Energy Environ. Sci.* **7**(3), 982 (2014).
42. F. Ma, J. Li, W. Li, N. Lin, L. Wang, and J. Qiao, "Stable  $\alpha/\delta$  phase junction of formamidinium lead iodide perovskites for enhanced near-infrared emission," *Chem. Sci. (Camb.)* **8**(1), 800–805 (2017).

## 1. Introduction

Metal halide perovskites have raised great interest due to their exceptional optoelectronic material properties, which can be translated into high-performance low-cost solution-processed devices [1,2]. Perovskite solar cells with efficiencies above 22% have been demonstrated after a short but intense research period; this performance now significantly exceeds that of other solution-processed materials [3]. The exceptional optoelectronic material properties also make them promising candidates for light emitting devices. Their superior charge carrier transport, higher index of refraction, and insensitivity of light emission on the spins of recombining charges (low triplet-exciton losses due to the dominant free carrier recombination) raise the possibility to overcome current challenges of solution processed lasers [4,5]. The more traditional materials in the field – such as conjugated polymers or colloidal quantum dots – are known for their superb color tunability and the ability for an easy integration into other devices and onto various substrates [6]. However, direct electrical pumping and their stability in operation are regarded as challenges that are hard to overcome [6–8]. Furthermore, with the exception of recent notable successes using colloidal nanocrystals [9–11], lasing under continuous-wave optical excitation also has proven difficult to achieve [12]. The fact that metal halide perovskites exhibit bipolar charge transport with much higher carrier mobilities, creates new hope to achieve a solution processed laser diode [13]. An overview over the recent efforts on perovskites lasers can be obtained by several review articles [4,14–16]. In the first report of optical gain in perovskites, Xing *et al.* demonstrated that the spectral position of optical gain could be tuned in principle by exchanging the halide [17]. Most of the following work on perovskite thin films concentrated on the workhorse composition for solar cells, methylammonium ( $\text{CH}_3\text{NH}_3/\text{MA}$ ) lead (Pb) triiodide ( $\text{I}_3$ ) that emits around 790 nm. Random lasers [18], whispering gallery mode lasers [19–22], distributed feedback lasers [23–25], vertical cavity lasers [26,27] and photonic crystals lasers have been demonstrated using this  $\text{CH}_3\text{NH}_3\text{PbI}_3$  composition [28,29].

The stability of triiodide perovskites was shown to be excellent [17,23], although hurdles still remain to achieving continuous-wave lasing [24,30]. Photophysical investigations of  $\text{CH}_3\text{NH}_3\text{PbX}_3$  with mixed-halides undertaken in the context of bandgap tuning for photovoltaics revealed that the emission wavelength and intensity of the mixed-halide material is highly unstable under illumination [31–33]. The reversible photoluminescence (PL) degradation most likely arises from ion motion within the material leading to a separation of the halides. Perovskites in which the  $\text{CH}_3\text{NH}_3$  cation is partially replaced by formamidinium ( $\text{CH}(\text{NH}_2)_2/\text{FA}$ ) show a similar behavior and different halide domains are formed in the films which results in broad emission spectra with multiple PL maxima [34]. Such properties of the mixed-halides clearly raise questions as to whether they are a suitable approach for tuning the amplified spontaneous emission spectra (ASE) of gain materials,

which is the fundamental prerequisite for lasing. However, the incorporation of a third cation in the form of cesium (Cs) was recently shown to suppress this halide segregation under illumination conditions relevant for photovoltaics giving new hope to enable continuous spectral tunability with a reasonable stability for mixed-halides [35].

In this paper, we investigate triple cation mixed-halide perovskites with regard to stability for optical gain applications and study the thresholds for ASE and the gain stability of these perovskites over a broad range as a function of the stoichiometry. We investigate perovskites emitting from 515 nm to 790 nm by exchanging the halides in small steps of 10%. Our samples exhibit narrow PL linewidths between 100 meV and 130 meV and exhibit optical gain over a wide spectral range. However, significant changes of the ASE thresholds and the stability depending on the stoichiometry are revealed.

## 2. Experimental techniques

### 2.1 Perovskite thin film preparation

Inspired by the preparation recipe by Saliba *et al.* [35], the perovskite precursors  $\text{PbX}_2$  (Alfa Aesar), CsX (Alfa Aesar), MAX (DyeSol) and FAX (DyeSol) with  $X = \text{I}, \text{Br}, \text{Cl}$  were dissolved in a mixture of dimethylformamide (DMF) and dimethyl sulfoxide (DMSO) in a ratio of 3:1 if not explicitly stated otherwise. The solutions were dynamically spin-cast at 1000 rpm for 10 s and 6000 rpm for 20 s on cleaned glass slides in nitrogen atmosphere. Five to seven seconds before the end of the process, 100  $\mu\text{l}$  of chlorobenzene were dropped onto the spinning sample. The samples were annealed at 100 °C for 60 minutes in  $\text{N}_2$ . The MA to FA ratio was held constant in all experiments to  $\text{MA/FA} = 1/5$  leading to an approximate stoichiometry of  $\text{Cs}_x(\text{MA}_{0.17}\text{FA}_{0.83})_{1-x}$  for the A cation in the precursor solution.

### 2.2 Optical characterization

For the PL and ASE measurements, the perovskites films were placed in an  $\text{N}_2$  atmosphere. Low band gap perovskite with an iodide content of 10% or more were excited with a 532 nm laser (CryLaS GmbH, FTSS355-Q2) emitting pulses with pulse length of 1 ns. Perovskites with no iodide content (and a higher band gap) were excited with a 355 nm pulsed laser (Advanced Optical Technology, AOT-YVO-20QSP), emitting pulses with pulse length of 0.5 ns. The emission was collected perpendicular to the samples through a dichroic mirror and analyzed in a spectrometer (Acton Research Corporation, SpectraPro) and a Peltier-cooled CCD camera (Princeton Research, PiMax). For the ASE stability measurements, an excitation energy corresponding to twice the initial ASE threshold energy for the respective sample was chosen. All experiments were performed at room temperature.

## 3. Results and discussion

### 3.1 ASE thresholds and stability

Saliba *et al.* recently demonstrated that the exact amount of Cs which replaces the methylammonium and formamidinium cations has a large effect on the efficiency and reproducibility of triple cation perovskite solar cells [35]. Starting from those findings, we begin by investigating the effect of different amounts of Cs on the optical gain characteristics. First, we use the same iodide content of 83% that Saliba *et al.* used for the realization of their highly efficient solar cells with power conversion efficiencies of >21% while maintaining very good operational and PL spectral stability [35].

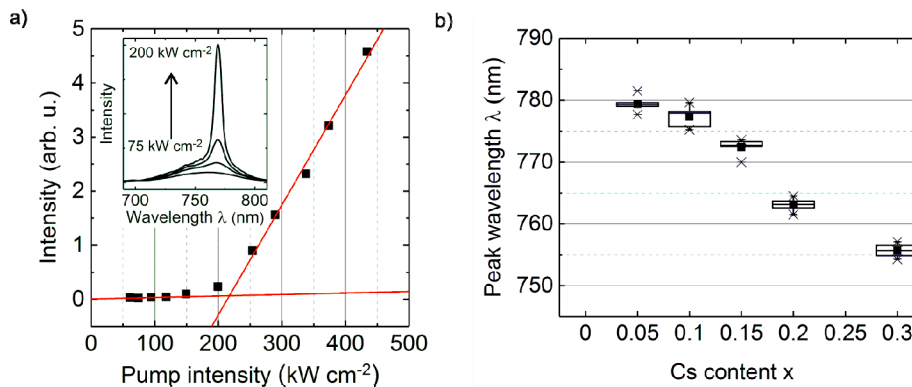


Fig. 1. a) Typical evolution of the peak intensity as a function of the pump intensity. Inset: Transition of the spectrum from PL to ASE. b) ASE peak wavelengths for different Cs contents  $x$  in perovskites films with the composition  $\text{Cs}_x(\text{MA}_{0.17}\text{FA}_{0.83})_{1-x}\text{Pb}(\text{I}_{0.83}\text{Br}_{0.17})_3$ .

We note that we do not add different amounts of stock solutions of CsI to the perovskite precursors solution as in the mentioned report, but we prepared separated solutions to maintain the exact stoichiometry for all samples. Figure 1(a) depicts a typical curve how the peak intensity increases as a function of the pump intensity for a triple cation sample. The inset indicates the evolution from PL to ASE. ASE thresholds were extracted by fitting linear slopes through the measurements points below and above the visible kink and calculating the intersection. The typical ASE signatures were not observed in binary perovskites containing only MA and FA as the cations (Cs-free perovskites). In contrast, all the Cs containing samples with the stoichiometry  $\text{Cs}_x(\text{MA}_{0.17}\text{FA}_{0.83})_{1-x}\text{Pb}(\text{I}_{0.83}\text{Br}_{0.17})_3$  with  $x$  ranging from 0.05 to 0.3 exhibited ASE with similar thresholds for all compositions (see the Appendix, Fig. 7). The increase in the Cs content, while keeping the halide ratio constant, also raised the bandgap of the material, shifting the peak ASE wavelength from 780 to 756 nm as can be seen in Fig. 1(b). This can be explained by the reduced ionic radius of Cs compared to MA and FA, which reduces the lattice constant and increases the bandgap [36]. Scanning electron microscopy (SEM) images do not show significant differences of the morphology within these compositions (see the Appendix, Fig. 8). The grain size is around 200 nm for all samples. We attribute the missing ASE in the Cs-free films to an incomplete crystallization for the applied fabrication protocol, which is supported by the greatly reduced steepness of the absorption onset in the films without Cs (see the Appendix, Fig. 9). We note that in principle ASE should also be achievable in binary perovskites with MA and FA, but we were not able to detect it here in the investigated fluence range. This supports the assumption that Cs assists in the crystallization process and adds a robustness to the fabrication processes as was also observed and described previously by Saliba *et al* [35].

Next, we investigated the role of the stoichiometric ratio between lead to the sum of all cations, since recent investigations have revealed a large influence of this parameter on the efficiency of solar cells [37,38]. The lead to cation ratio (Pb/A) is defined as the ratio of the number of lead (Pb) anions divided by the sum of the three A cations (number of MA molecules + number of FA molecules + number of Cs cations) in the precursor solution. Figure 2(a) shows the ASE thresholds for various lead to cation ratios. There is a clear trend to lower thresholds for a moderate deficiency of lead. For the lowest Pb/A ratio of 0.8, the thresholds were lowest if ASE occurred, but not all of the films with this ratio exhibited ASE. The Pb/A ratio also has a major impact on the morphology as can be seen in the SEM images in Fig. 2(b).

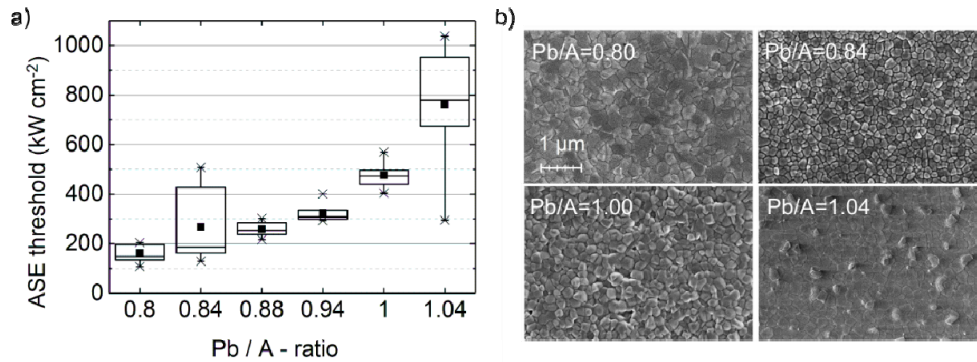


Fig. 2. Influence of different stoichiometric ratios on a) the ASE thresholds and b) the morphology. Pb/A is the ratio of the number of lead (Pb) atoms to the sum of the three A cations (number of methylammonium (MA) molecules + number of formamidinium (FA) molecules + number of cesium (Cs) cations) in the precursor solution.

Films with a Pb/A ratio of 0.8 are smooth, but do not show well defined grain boundaries. For a ratio of 0.84 the individual crystals are better visible and clear grain boundaries can be seen. For higher lead contents, there are well defined crystals with a higher overall roughness. If an excess of lead is present in the precursors solution, some crystals are sticking out of the film. An increased roughness for higher Pb contents can also be seen by the stronger diffuse scattering of the samples (see the Appendix, photograph Fig. 10). For optical gain in thin films, a smooth layer is preferable since the waveguide mode exhibits less scattering leading to a higher modal gain [39]. The better gain performance in these perovskites with a deficiency of lead is in contrast to perovskite solar cells, where a lead excess was found to improve the efficiency [37,38]. Jacobsson *et al.* recently suggested that a lead excess is improving charge carrier transport through grain boundaries while the overall crystal quality suffers, however, with a net positive effect for solar cells [38]. Since charge carrier transport is less important in our optically pumped devices, the better crystal quality together with the smoother surface can explain the lower ASE thresholds. For best reproducibility and low thresholds, we continued to work with a Pb/A value between 0.84 and 0.88 and Cs content of 10-15%. An annealing temperature of 90-100°C for a duration of 60 minutes was found to be optimal for this composition (see the Appendix, Fig. 11 and corresponding annotations).

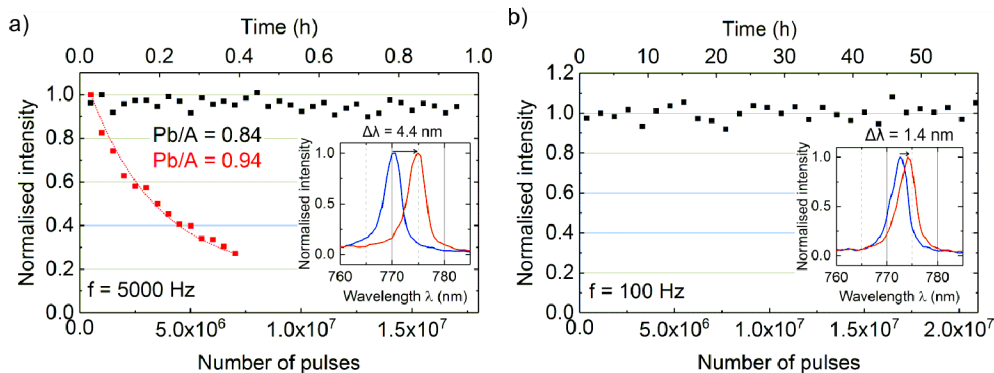


Fig. 3. a) Comparison of the stability for different stoichiometric ratios at 5 kHz repetition rate. b) At a low repetition rate of 100 Hz, the ASE wavelength red-shift is significantly reduced. Insets: Normalised spectra of the first (blue) and of the last (red) spectrum.

While the stability of single-halide perovskites with methylammonium as the cation is typically very good under excitation conditions necessary for ASE [14,20], mixed-halides materials degrade even under low excitation conditions very quickly with the peak emission

shifting to longer wavelengths within seconds [31]. Figure 3(a) compares the ASE stability of this triple cation perovskites with different Pb/A ratios. We find that perovskites with the same deficiency of lead, which resulted in the lowest ASE thresholds, had greatly superior performance. For perovskites with a Pb/A ratio of 0.94, the emission intensity drops in less than 20 minutes to half of its initial intensity. In contrast, perovskites with a Pb/A ratio of 0.84 exhibit a stable emission intensity for over 1 hour at a repetition rate of 5 kHz, corresponding to  $1.8 \times 10^7$  pulses. Further testing showed that this composition maintains very stable emission intensity over 2 days at 5 kHz corresponding to more than  $8 \times 10^8$  pulses, although there is some drift to longer wavelengths of the ASE peak (see the Appendix, Fig. 12). These findings are consistent with recent investigations by Liu *et al.*, who observed that remnant  $\text{PbI}_2$  in perovskite thin films is accelerating the degradation of perovskite solar cells [40]. Although it was reported that triple cation solar cells do not show any emission wavelength red-shift under illumination conditions relevant to solar cells, we observe red-shifting of the emission with time at the high excitation densities necessary for ASE. Even for our perovskite with a very stable emission intensity, we see a small red-shift of 4.4 nm within 1 hour of excitation at a repetition rate of 5 kHz. In the two days long-term measurement at high repetition rate of 5 kHz, the ASE peak wavelength shifts by 19.2 nm with continuous slowing down of the red-shift over time (see the Appendix, Fig. 12(b)). The PL red-shift has been attributed to a halide segregation, which occurs under illumination [31–33]. Thus, this process depends on the specific excitation conditions. When a low repetition rate of 100 Hz is used for the stability test, the spectral position of the ASE Peak only shifts by 1.4 nm after 20 million pulses, corresponding to 55 hours of operation as is depicted in the inset of Fig. 3(b). We are confident that a further material optimization and/or a lowering of the thresholds – for example by post-structuring of the perovskite layers [29] – will eliminate the halide segregation and prevent the wavelength shift in future perovskite devices for lasing applications.

### 3.2 Bandgap tuning

For light emitting applications, one of the most interesting features of metal-halide perovskites is the ability to tune the bandgap by exchanging the halide. For perovskites employing only methylammonium, formamidinium or a mixture of both as cations, sharp absorbance onsets and single narrow emission peaks cannot be maintained over the whole spectral region accessible by tuning the ratio of iodide and bromide [31,34,41]. Thus it is important to note that we can achieve sharp absorption onsets and narrow emission peaks over the entire range of ratios using our triple cation perovskites. As can be seen in Fig. 4(a) we steadily tune the PL from peak wavelengths of 510 nm to 790 nm by exchanging the halides in steps of 10% while preserving narrow PL spectra and sharp absorption edges (see the Appendix, Fig. 13) throughout the whole spectral region. Figure 4(b) depicts the ASE spectra achieved through halide tuning. We observe ASE at peak wavelengths between 545 nm to 555 nm ( $\text{Cl}_{0.1}\text{Br}_{0.9}$  and  $\text{Br}_{1.0}$ ) and then between 680 nm to 810 nm ( $\text{Br}_{0.5}\text{I}_{0.5}$  to  $\text{I}_{1.0}$ ). For achieving ASE in thin films of  $\text{Br}_{0.5}\text{I}_{0.5}$  we needed to use a mixing ratio of DMF:DMSO of 1:1 instead of 3:1 as for the other compositions in order to change the crystallization dynamics. Photographs of the samples corresponding to the emission spectra are depicted in Fig. 4(c). The full width at half maximum (FWHM) of the PL is between 100 meV to 130 meV throughout the entire range as depicted in Fig. 5(a). This spectral linewidth is in agreement to literature reports of pure iodide and bromide films [40–42]. The similar FWHM for all the mixed-halide perovskites reflects the homogenous distribution of the halides for all mixing ratios without separated halide domains in the films.

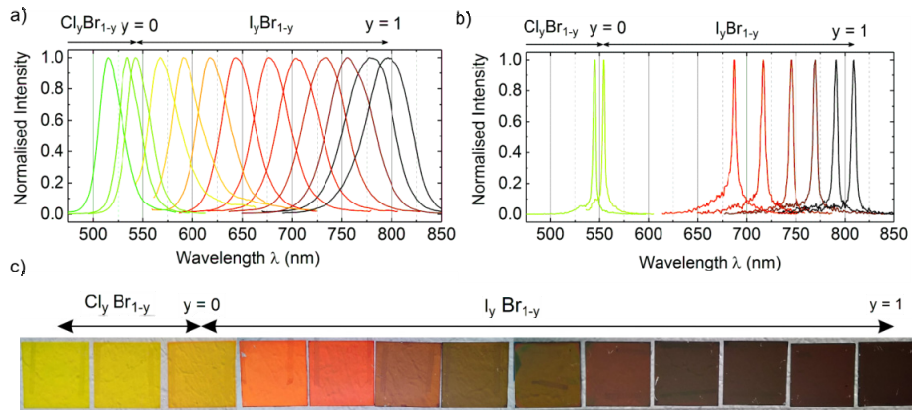


Fig. 4. a) PL spectra of triple cation perovskites with halide compositions ranging from  $\text{Cl}_{0.2}\text{Br}_{0.8}$  to  $\text{I}_{1.0}$ . b) ASE spectra of the samples where optical gain was achieved in the investigated fluence range. c) A photograph of the samples corresponding to the emission spectra in a).

The FWHM of the ASE spectra were measured to be around 10 meV to 13 meV for all compositions. Figure 5(b) shows the ASE peak wavelength in dependence of the halide composition. There is a small deviation from a linear dependency of the ASE peak as function of wavelength as well as a function of photon energy. The ASE thresholds for the different compositions are shown in Fig. 5(c). They are lowest for iodide rich perovskites for which the fabrication protocol was optimized. The pure bromide material also exhibited a threshold value of around  $250 \text{ kW/cm}^2$ .

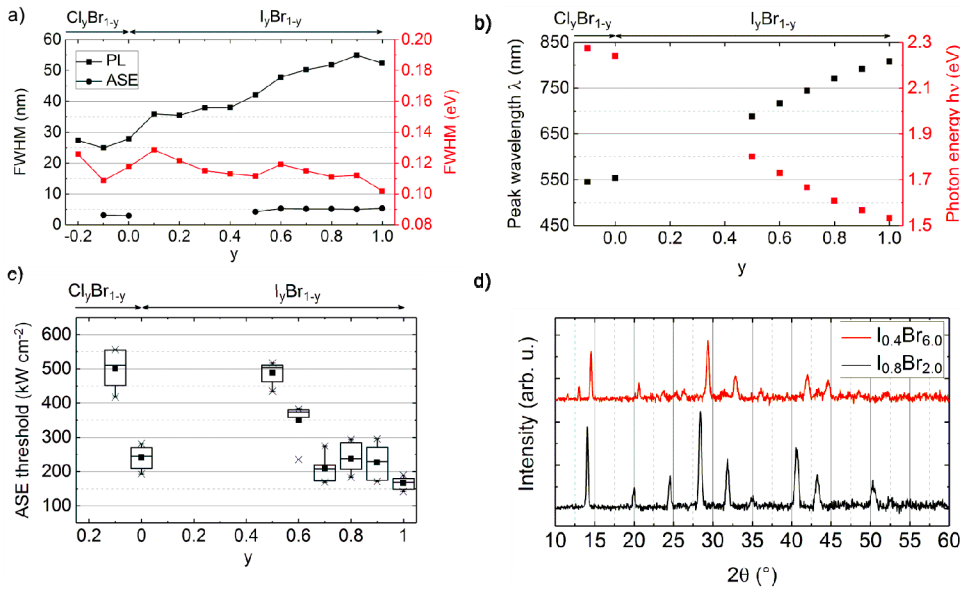


Fig. 5. a) FWHM of the PL and ASE spectra for triple cation perovskites with different halide ratios. b) ASE peak wavelengths in dependence of the halide composition. c) ASE thresholds for different halide compositions. d) XRD patterns of  $\text{I}_{0.8}\text{Br}_{0.2}$  (exhibiting ASE) and  $\text{I}_{0.4}\text{Br}_{0.6}$  (not exhibiting ASE).

However, for the materials in the range of  $\text{I}_{0.1}\text{Br}_{0.9}$  to  $\text{I}_{0.4}\text{Br}_{0.6}$  we do not observe ASE (in the investigated fluence range). We attribute the lack of ASE in this region and the difference in the ASE thresholds to be primarily due to incomplete crystallization for some mixtures. Figure 5(d) shows XRD patterns of  $\text{I}_{0.8}\text{Br}_{0.2}$  and of  $\text{I}_{0.4}\text{Br}_{0.6}$ . While all the peaks in the sample

with 80% iodide matches to the  $\alpha$ -perovskite phase, the additional small peaks at  $11.6^\circ$  and  $13.05^\circ$  in the sample with 40% iodine can be attributed to the  $\delta$ -phase of  $\text{FAPbI}_3$  and to  $\text{PbI}_2$ , respectively [35,42]. SEM images show a different surface morphology for the different composition supporting this assumption (see the Appendix, Fig. 14). For high bromide fractions where the ASE thresholds are high or no ASE is observed, the grain boundaries are less well visible and tend to merge indicating that the process of crystallization is not optimal. In comparison, films with high iodide content and low ASE thresholds show well-defined crystals and grain boundaries.

We now turn to a discussion of the stability for the different bandgap materials. Figure 6 depicts the ASE stability of all compositions in which ASE was achieved. While the intensity stability is excellent for perovskites with high iodide contents for which we optimized our fabrication protocol, the stability gets worse starting from 40% bromide content. Perovskites with only bromide also exhibit excellent stability, but the introduction of chloride in order to tune to shorter wavelengths decreases the stability significantly. There is a clear correlation between the stability and the ASE threshold, which we assume to arise partly from a different crystallization quality and the higher pumping fluences for those compositions (as mentioned above, all stability experiments were done at twice the initial threshold fluence). The amount of peak wavelength red-shift per hour increases approximately linear with the mixing ratio (see the Appendix, Fig. 15). Again, further work to improve the crystal quality of these materials should improve their ASE thresholds and stability.

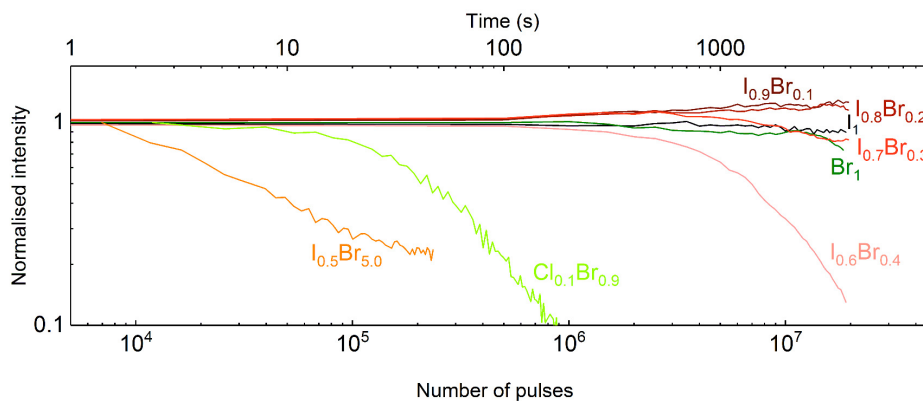


Fig. 6. ASE emission intensity stability for different halide compositions.

#### 4. Conclusions

We have shown that triple cation perovskites provide a route to obtaining stable optoelectronic materials with well-defined bandgaps allowing the gain spectra to be tuned over a wide spectral range. We found that it is crucial for lowering the ASE threshold and increasing the stability under intense optical excitation to add Cs and to use a moderate deficiency of Pb in the precursor solutions. For high iodide contents and pure bromide perovskites, no degradation of the ASE intensity is observable for more than 10 million pulses. However, at the intense pumping conditions needed to obtain ASE (and consequently high charge carrier densities), a slow phase segregation of the halides still occurs. This segregation depends on the excitation conditions and can be slowed down, for example, by reducing the excitation repetition rate. With a halide exchange in steps of 10% from pure iodide to pure bromide and with further incorporation of up to 20% chloride, we could tune the PL between 510 nm to 790 nm while preserving a FWHM of the PL between 100 meV to 130 meV across the whole range. ASE was observed over a wide portion of this range, although it was not achieved in some of the mixed-halides due to an incomplete crystallization. We conclude that triple cation perovskites are enabling wide tuning of the

ASE spectrum. With further individual optimization of the fabrication protocols for different compositions and/or the incorporation of other ingredients, low threshold ASE from the visible to the near infrared based on the control of halide ratio should be achievable under ns excitation. The tunable emission and ASE characteristics combined with the excellent stabilities over a wide wavelength range demonstrated in this work suggest a bright future for perovskite light emitting devices.

## 5. APPENDIX – Additional figures

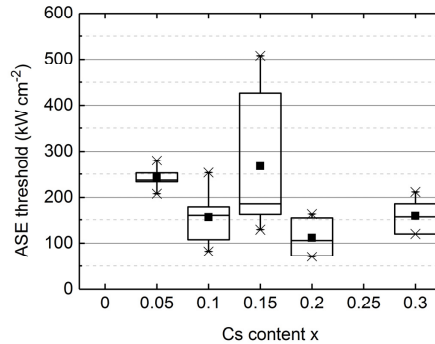


Fig. 7. ASE thresholds for different amounts of Cs in  $\text{Cs}_x(\text{MA}_{0.17}\text{FA}_{0.83})_{1-x}\text{Pb}(\text{Br}_{0.17}\text{I}_{0.83})_3$  perovskites. No ASE was detected in films without Cs for the applied fabrication protocol.

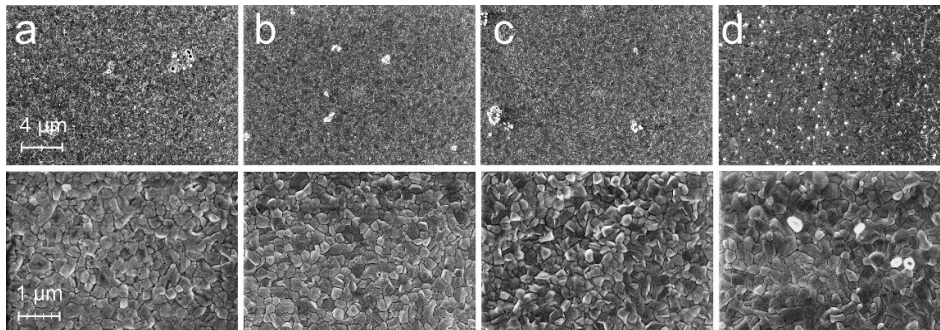


Fig. 8. SEM images of  $\text{Cs}_x(\text{MA}_{0.17}\text{FA}_{0.83})_{1-x}\text{Pb}(\text{Br}_{0.17}\text{I}_{0.83})_3$  perovskite films with different Cs contents x: (a)  $x = 0$ , (b)  $x = 0.1$ , (c)  $x = 0.2$  (d) and  $x = 0.3$ .

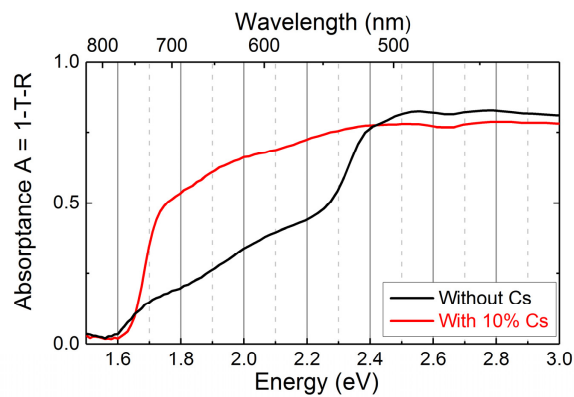


Fig. 9. Absorbance spectra of triple cation perovskites  $\text{Cs}_x(\text{MA}_{0.17}\text{FA}_{0.83})_{1-x}\text{Pb}(\text{Br}_{0.17}\text{I}_{0.83})_3$  films with ( $x = 0.1$ ) and without addition of Cs ( $x = 0$ ). Without Cs the films show a less steep bandgap which indicates an incomplete crystallization.

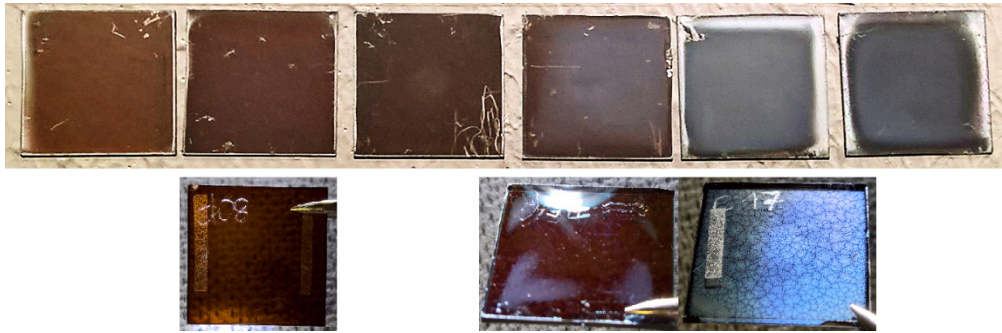


Fig. 10. Photograph of films with different stoichiometric ratios. On the top row, the Pb/A ratio from left to right is: 0.8, 0.84, 0.88, 0.94, 1 and 1.04. The bottom row shows photographs made from the backside of the films with ratios Pb/A of 0.84, 0.94 and 1.

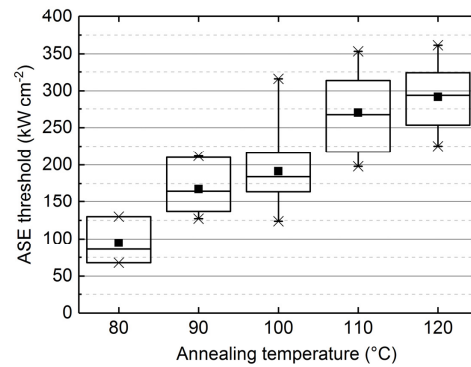


Fig. 11. ASE thresholds of perovskites for different annealing temperatures and a stoichiometry of  $\text{Cs}_{0.15}(\text{MA}_{0.17}\text{FA}_{0.83})_{0.85}\text{Pb}_{0.88}(\text{I}_{0.84}\text{Br}_{0.16})_{2.76}$ . Note: Not all of the films annealed at 80°C exhibited ASE.

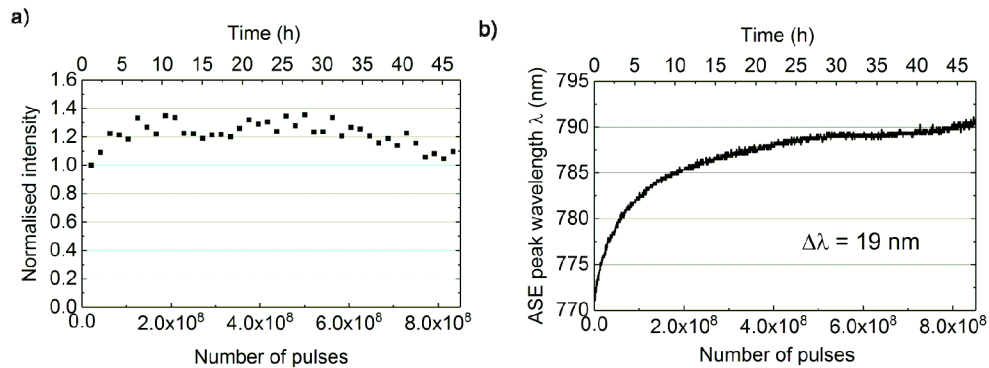


Fig. 12. Long term stability measurements under continuous illumination at 5 kHz of perovskites with stoichiometry  $\text{Cs}_{0.15}(\text{MA}_{0.17}\text{FA}_{0.83})_{0.85}\text{Pb}_{0.88}(\text{I}_{0.83}\text{Br}_{0.17})_{2.76}$ : a) Maximum intensity b) ASE peak wavelength.

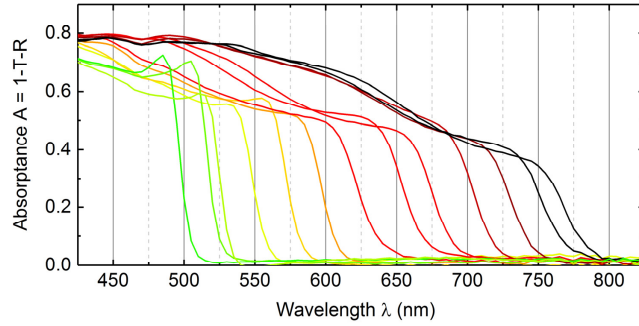


Fig. 13. Absorbance spectra of the films with halides ranging from I<sub>1</sub> to Br<sub>0.8</sub>Cl<sub>0.2</sub>.

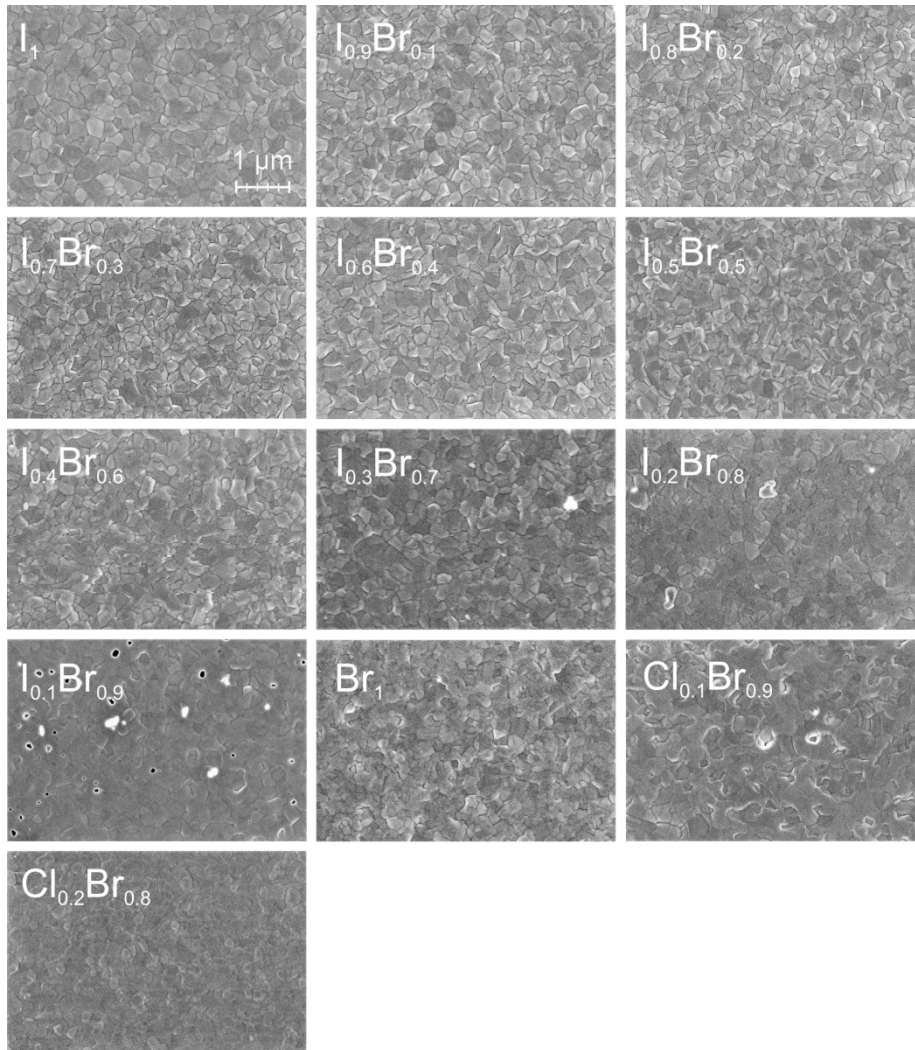


Fig. 14. SEM images of perovskites with different halide compositions.

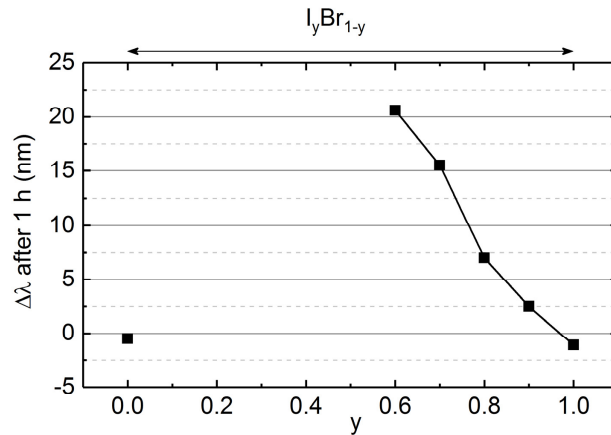


Fig. 15. ASE peak wavelength red-shift per hour for different halide compositions.

### Funding

Deutsche Forschungsgemeinschaft (DFG) (LE 878/17-1).

### Acknowledgments

We thank S. Habermehl and V. Schendel for SEM measurements. P. Brenner, D. Rueda, T. Abzieher and M. Jakoby acknowledge support by the Karlsruhe School of Optics & Photonics (KSOP). We acknowledge support by Deutsche Forschungsgemeinschaft and Open Access Publishing Fund of Karlsruhe Institute of Technology. The authors would also like to gratefully acknowledge the Initiating and Networking funding of the Helmholtz Association (HYIG of Dr. U.W. Paetzold; Rekrutierungsinitiative Prof. B.S. Richards) and the Helmholtz Energy Materials Foundry for financial support.